JMEPEG (2009) 18:484–489
DOI: 10.1007/s11665-009-9398-6

1059-9495/$19.00

# Processing of Shape Memory CuZnAl Open-cell Foam by Molten Metal Infiltration

*E.M. Castrodeza, C. Mapelli, M. Vedani, S. Arnaboldi, P. Bassani, and A Tuissi*

*(Submitted October 15, 2008; in revised form January 26, 2009)*

**Foams and other highly porous materials with a cellular structure are known to have many interesting combinations of physical and mechanical properties. In addition, foaming of shape memory alloys (SMA) greatly improves the set of application possibilities. In this work an open-cell metal foam of a CuZnAl SMA is presented. This foam was produced through a recently proposed process, which consists mainly in molten metal infiltration of a bed of silica-gel particles and the subsequent use of hydrofluoric acid (HF) as solvent. The results showed that very regular open-cell foams could be obtained, having an almost spherical cell morphology and relative densities of approximately 0.3. Microstructural and compositional analyses on foamed specimens showed uniform microstructure of ligaments and the absence of $SiO_2$ interaction with the metal. In this way the possibility of foaming CuZnAl system through the proposed low-cost process was clearly demonstrated.**

**Keywords** cellular materials, CuZnAl, metal foam, shape memory alloys

## 1. Introduction

### 1.1 Metal Foams

The unique combination of morphology and material in cellular metals offers an interesting set of physical-chemical and mechanical properties that makes these materials very attractive both for structural and functional applications. Cellular metals can be produced by several processes that include molten metal infiltration in a particular leachable bed of solid particles (Ref 1-4).

This work introduces the use of an amorphous $SiO_2$ (silica-gel) bed as space holder for open-cell CuZnAl shape memory alloy (SMA) foam production through molten metal infiltration. Once infiltrated, $SiO_2$ particles are dissolved by a wet solution of hydrofluoric acid (HF). By this route, highly homogeneous foams of CuZn alloys, having almost spherical open-cell morphologies, can be produced (Ref 5, 6). The proposed methodology was based on cheap commercial consumables and a simple technology, focusing on intermediate-density low-cost foams with interesting cost/benefit ratios.

Metal foams obtained by liquid infiltration of leachable space holder are usually Al-based. In this case, NaCl particles leached by pure water are used (Ref 1, 2, 4, 6-8). More recently, open-cell amorphous metal foams were processed using refractory fluoride salts (Ref 9). No matter the mineral salt used for metal foaming, all the reported materials have melting point lower than $SiO_2$, being this a limitation for the application of the route to high melting point metals and alloys. Besides, due to the irregular morphology of mineral salt particles, the final products have mainly irregular cell morphologies, even if good cell distribution and size are obtained (Ref 4, 7, 9).

The use of $SiO_2$ beads as space holder results in cellular metals with a very homogeneous arrangement of almost spherical cavities. Additionally, because of the high chemical stability of $SiO_2$, reactions between space holder and molten metal tend to be minimal or inexistent.

### 1.2 CuZnAl Shape Memory Alloys

Among the large number of SMAs which have been discovered, most are copper-based. The most known NiTi SMAs exhibit better properties in strength, ductility and resistance to corrosion, in addition to excellent SME characteristics, but they are very expensive compared with Cu-based SMAs. Hence, two groups of cheap Cu-based alloys are currently being developed: Cu-Al based and Cu-Zn-X ternary alloys. Among ternary alloys, the Cu-Zn-Al system has often been the subject of research (Ref 10, 11).

The studies on this system have been mainly focused on shape memory and superelastic effect, aging phenomena and fatigue properties (Ref 12-18). Corrosion resistance was seldom examined (Ref 19). Due to the relative low melting temperature, these SMAs are easy to manufacture and have excellent electric performance, heat conductivity and a strong memory effect. Cu-based SMAs are in general also prone to

This article is an invited paper selected from presentations at Shape Memory and Superelastic Technologies 2008, held September 21-25, 2008, in Stresa, Italy, and has been expanded from the original presentation.

**E.M. Castrodeza, C. Mapelli,** and **M. Vedani**, Dipartimento di Meccanica, Politecnico di Milano, Via G. La Masa 34, 20156 Milan, Italy; **E.M. Castrodeza**, Departamento de Ingeniería de Materiales, Universidad de Concepción, Edmundo Larenas 270, 4070409 Concepcion, Chile; and **S. Arnaboldi**, **P. Bassani**, and **A Tuissi**, CNR-I-ENI, Unità di Lecco, Corso Promessi Sposi 29, 23900 Lecco, Italy. Contact e-mails: sergio.arnaboldi@ieni.cnr.it, and tuissi@ieni.cnr.it.

aging effects and show excessive grain growth when heat-treated (Ref 20, 21). These phenomena cause the well-known and unwanted problems, such as martensite stabilization or intergranular cracking, that hindered a wider diffusion of these alloys in the past decades. However, all the studies carried out in recent years seem to confirm that innovative applications by the use of these materials are feasible and well promising.

## 2. Experimental

### 2.1 Shape Memory Alloy Foaming

In this work the tested material was a typical CuZnAl SMA. The chemical composition and some physical properties of the alloy are reported in Table 1. The SMA was cast in an Aseg Galloni VCMIII induction melt casting machine, under pure Ar flow at room pressure. The maximum electrical power of this machine is 6 kW and it is equipped with a cylindrical graphite crucible of approximately 250 ml. A small cylinder of SMA having almost 30% of the intended foam volume was placed at the bottom of a vertical graphite crucible (80 mm in depth, 60-mm internal diameter). Then a bed of silica-gel beads was placed on the top of the SMA cylinder, also inside the crucible, and gently shaken for improving piling. Finally, a short cylindrical piece of graphite was positioned on top as a cap, closing the crucible for better temperature distribution over the silica beads. This initial configuration can be seen on Fig. 1(a). At this point the inductor was turned on and after some minutes, the metal was molten. During the melting, the metal temperature was continually measured by the thermocouple positioned in a blind hole in the solid SMA cylinder. After complete melting, when approximately 100 °C overheating was reached, the crucible cap and thermocouple were retired, the induction main power was turned off and silica-gel bed was pressed down by a steel cylinder having 85 N in weight (Fig. 1b and c). The infiltrated metal was at this point able to solidify between the silica particles (Fig. 1d). After complete solidification and cooling, the remaining solid (silica-gel beads plus infiltrated SMA) was unmolded and lathe machined to its final shape. Finally, the piece was submerged in an aqueous HF bath (25 vol.%) till complete $SiO_2$ dissolution was achieved.

The material was heat treated in a resistance furnace and quenched in water at room temperature (betatization treatment). In order to investigate the best condition for betatization, heat treatments with different temperatures and times were carried out.

The relative density of the final foam, the ratio of foamed to bulk material density, was theoretically calculated based on the bulk SMA density (Table 1), on weight measurements of the samples and on careful measurements of physical dimensions of the final (post-machined) cellular solid.

During the different steps of the whole process, material samples were collected and characterized. Calorimetric analyses were performed in a Seiko SCC/5200 differential scanning calorimeter at a rate of 10 °C/min in a range −100/80 °C which includes the direct and reverse transformations. The specimens were metallographically polished and etched with an alcoholic solution of $FeCl_3$. The material microstructure and its composition were investigated using a conventional optical microscope and a scanning electron microscope, equipped with energy dispersive spectroscopy (EDS) microanalyses system.

### 2.2 Amorphous $SiO_2$ (Silica Gel) Beads

Commercial non-indicating Sigma S7500 silica-gel Type II beads were used. The chemical composition of the particles and some of their physical properties are summarized in Table 2. Synthetic amorphous silica is virtually inert and has no known

**Table 1 Chemical composition and physical properties of the investigated alloy**

| Chemical composition, wt.% | | | Physical properties | |
|---|---|---|---|---|
| Cu | Zn | Al | Melting temperature, °C | Density, g/cm$^3$ |
| 72.5 | 21.5 | 6 | 920 | 8.16 |

**Table 2 Typical properties of the used silica-gel beads**

| Composition | Average diameter, mm | $SiO_2$ density, g/cm$^3$ | Bead density (bulk), g/cm$^3$ | Melting point, °C | Boiling point, °C |
|---|---|---|---|---|---|
| $SiO_2 > 99.7\%$ | 3.175 | 2.2 | 0.7 | ~1600 | 2230 |

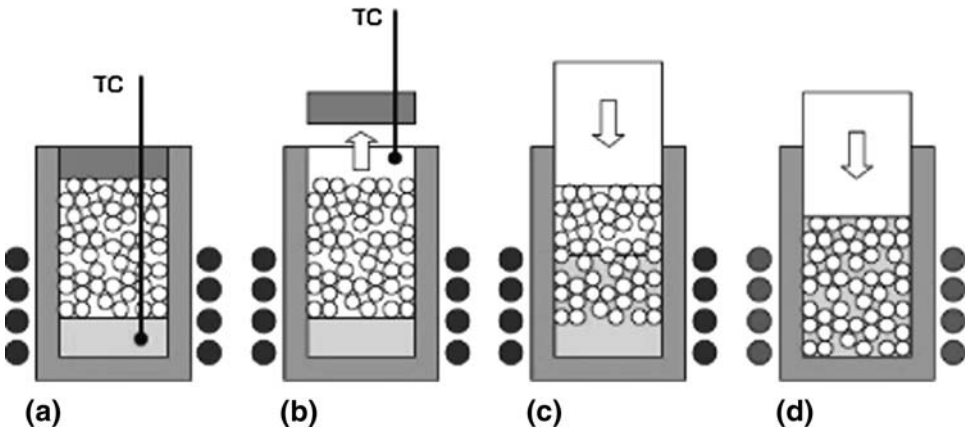


**Fig. 1** Schematic of the infiltration process

adverse effects on the environment. This material is normally used as desiccant and it is commercially available worldwide as a cheap commodity.

The silica-gel beads were treated before infiltration to remove humidity content at 200 °C for 1 h and then heat treated in air at 900 °C for approximately 45 min.

### 2.3 Wet Chemical Etching of Silica-gel

Silica-gel was dissolved by wet chemical etching in aqueous solution of HF (25 vol.%). In literature it is possible to find several proposed reactions for HF etching of $SiO_2$. The stoichiometric reaction is defined as (Ref 22):

$$4HF + SiO_2 \leftrightarrow SiF_4 + 2H_2O.$$

Having aqueous HF in excess (as for our case) the main chemical reactions seems to be (Ref 23):

$$SiO_2 + 6HF \rightarrow H_2SiF_6 + 2H_2O,$$

and

$$SiO_2 + 3HF_2^- + H^+ \rightarrow SiF_6^{2-} + 2H_2O.$$

It must be specified that the highly porous morphology of silica-gel particles and the stirring action of the HF solution make the etching of beads rather easy.

## 3. Results and Discussion

### 3.1 Process

A little batch of CuZnAl foams were produced in order to evaluate feasibility and reproducibility of the process. EDS microanalyses show an excellent mean homogeneity of the chemical composition. A resulting cylindrical piece of metal and silica-gel beads after solidification and external lathe machining is shown in Fig. 2. The irregular face on the right of Fig. 2 corresponds to the upper side of the crucible. Figure 3 shows a SEM image of a heat treated and polished specimen surface. In both images the infiltrated silica-gel beads can be clearly seen. Figure 4 shows the final sample of the CuZnAl foam after silica-gel dissolution. Figure 5 shows a SEM image of the polished specimen surface. It is possible to see the uniform pore distribution of almost spherical cells, as well as many interconnecting windows.

As can be seen from Fig. 4 and 5, silica-gel beads were completely dissolved by HF, without optical evidence of any significant metal corrosion. From these images it is possible to see that the silica-gel beads remained in the initial shape and size during metal infiltration. SEM and EDS analyses show no reactions products or inter-diffusive phase between metal and space holder spheres and no traces of Si and O on metal ligaments after $SiO_2$ leaching. This behavior was expected and it is in accordance to the mechanical and chemical stability of $SiO_2$ beads at the processing temperature selected (maximum processing temperature 1050 °C). The inner surface of the open cells shows the "negative image" of the surface morphology of pre-heated silica-gel beads.

Density calculations for the final foam specimen of Fig. 4 led to a relative density of 0.31 (corresponding to 69% of empty space). Empty space proportion is slightly higher than the reported 63-64% that corresponds to random packing of shacking hard spheres of the same size (Ref 24).

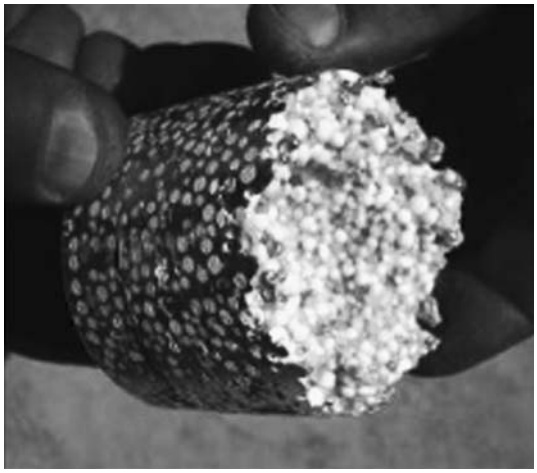

**Fig. 2** Infiltrated $SiO_2$ beads after cooling and external lathe machining

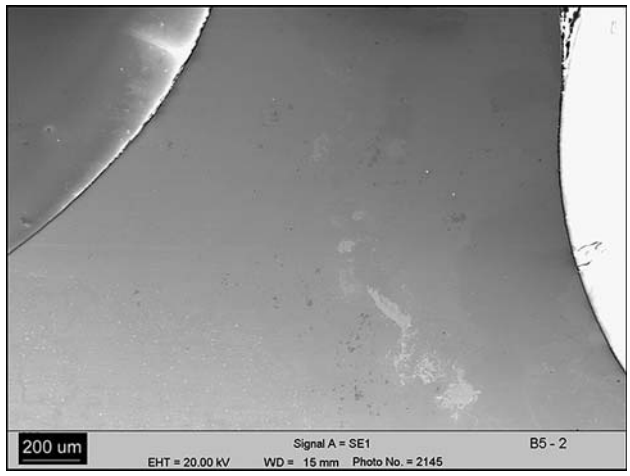


**Fig. 3** SEM image of a heat-treated and polished specimen surface

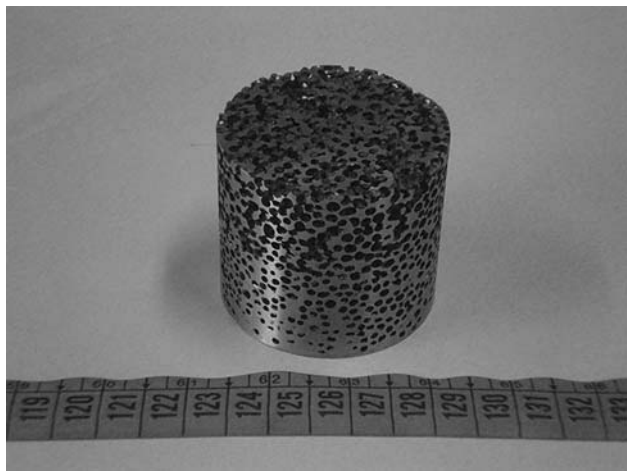

**Fig. 4** Final sample of foam after machining and $SiO_2$ dissolution

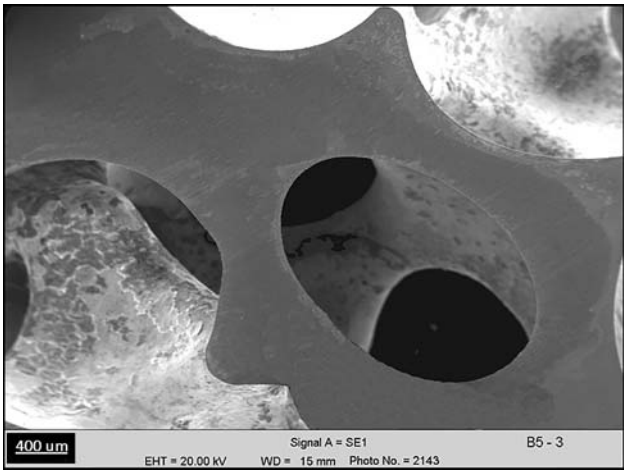


**Fig. 5** SEM image of a polished specimen surface

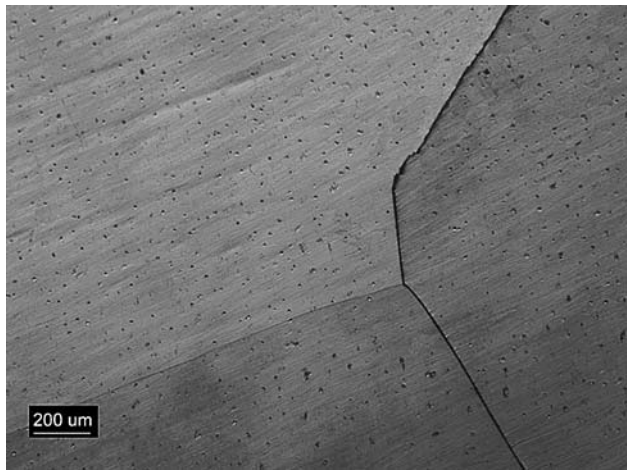


**Fig. 6** Representative images of the betatized bulk microstructure

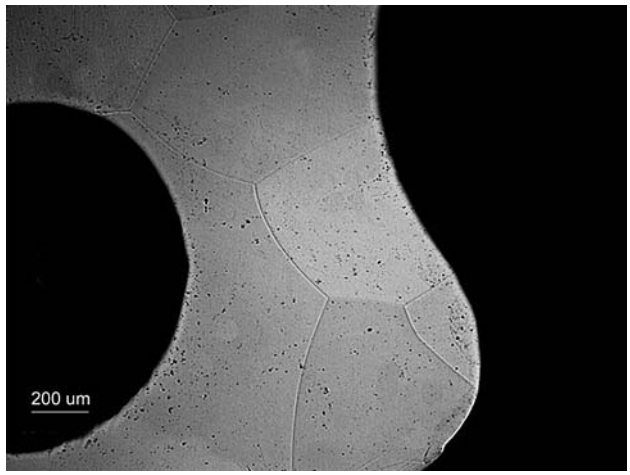


**Fig. 7** Representative images of the betatized foam microstructure

This result could be partially explained as a result of the non-complete wettability of silica-gel beads by molten brass that leaves part of the interstitial space unfilled, counterbalancing some piling faults and also permitting the existence of these small interconnection windows between silica-gel beads (Ref 4). Other reasons for this positive deviation of the theoretical space holder volume are (Ref 24, 25): (a) silica-gel beads are not perfectly spherical, (b) their size is not uniform, and (c) there is a localized contraction of the metal during the solidification.

No matter the contribution of each mechanism, the wettability of silica-gel beads by molten metal plays an important role in the process (Ref 4). If silica-gel beads were completely wetted by molten brass the interconnection windows would be very small or inexistent and dissolution of the space holder could be harder or even not possible. Although metal infiltration of porous space holders depends on many other variables (i.e., metal pressure, infiltration velocity, etc.) (Ref 1-4) the study of those influences was beyond the scope of the work.

As for other production processes of metal foams, the proposed route has some dimensional limitations and is non-continuous, batch method. The achievable relative density of the metal sponges seems to be in the range 0.25-0.35, depending mainly on silica-gel morphology (i.e., irregular and/or almost spherical particles) and granulometric distribution. These features are common to processes that use leachable particles as space holder (Ref 1, 2). The main difference of the proposed process is the suitability of the space holder for higher temperatures. Non-indicating silica-gel (very stable silicon oxide $SiO_2$) is non-toxic and commonly used in drugs and food industries. On the other hand, the use of HF in the proposed process seems to have the same limitations and regulations that in the semiconductor industry, which also uses HF for $SiO_2$ leaching.

### 3.2 Microstructure and Transformation Behavior

In as cast condition the alloy microstructure is made up by a mixture of alpha and beta-phases. After heat treatment at 830 °C for 15 min and water quenching (Fig. 6 and 7), a single-phase microstructure is evident both in bulk and foamed specimens. The grain size grew up to 2 mm in the bulk material during the betatization. It is also possible to notice that the grain growth in the foamed materials is less evident. This phenomenon could be due to the different cooling conditions during the quench in the foamed and in the bulk material. Moreover, the geometrical limitation in the foamed state could slow down the grain growth rate. No alpha precipitates can be observed at grain boundaries and the microstructure shows only localized martensite plates.

**Table 3 Bulk material DSC results after betatization treatment**

| $M_s$, °C | $M_f$, °C | ΔH, mJ/mg | $A_s$, °C | $A_f$, °C | ΔH, mJ/mg |
|---|---|---|---|---|---|
| −7.6 | −12.5 | −5.6 | −5.7 | −1 | 5.9 |

The transformation behavior was investigated by DSC measurements. The values reported in Table 3 and 4, show transformation temperatures lower than room temperature with comparable values in both specimens. In the reference bulk betatized state, the investigated alloy has a sharp transformation peak, which is depicted in Fig. 8. In this condition Ms, ΔH, and hysteresis are derived (Table 3). DSC scans of the foamed alloy in as cast condition, after betatization and after dissolution of silica-gel beads, are reported in Fig. 9. It is possible to observe

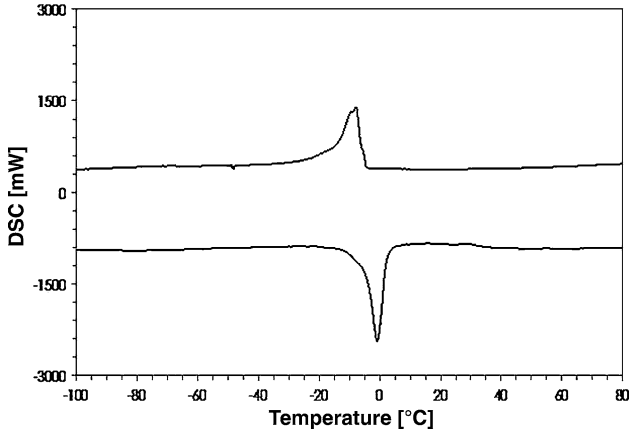


**Fig. 8** DSC profiles of betatized bulk specimens

**Table 4 Foamed material DSC results**

| State | $M_s$, °C | $M_f$, °C | ΔH, mJ/mg | $A_s$, °C | $A_f$, °C | ΔH, mJ/mg |
|---|---|---|---|---|---|---|
| As cast | −19.2 | −86 | −3.5 | −40.7 | −7 | 3.9 |
| Betatized (before dissolution) | −9.2 | −20 | −5.8 | −7.9 | 1.4 | 6.2 |
| Betatized (after dissolution) | −2 | −27.3 | −6 | −10.2 | 7.9 | 6 |

that betatization treatment promotes the transformation behavior and DSC peak in the same temperature range of the bulk material is detected. After dissolution a broader double peak is observed in the temperature range reported in Table 4. The changes in the transformation behavior, is likely to be connected to intrinsic inhomogeneities of the DSC specimens, taken from different positions in the foamed SMA. In fact, possible variation in the microstructure or morphology of the analyzed DSC samples may affect more peak intensity and shape than onset and offset transformation temperatures. Moreover, residual internal mechanical stresses, that could araise in the foamed SMA during its water quench and change after the dissolution of the silica-gel beads, may vary the peak intensity and subsequently the transformation enthalpy.

## 4. Conclusions

Based on experimental results it is possible to draw the following conclusions.

1. The production of metal foams of CuZnAl SMAs by molten metal infiltration of silica-gel beads, subsequently leached by aqueous HF was experimentally demonstrated.
2. Silica-gel remains stable in shape and dimensions during liquid-brass infiltration (maximum processing temperature 1050 °C). Due to the high chemical stability of $SiO_2$ particles, no interaction with the metallic system during liquid infiltration was found.
3. Silica-gel beads are completely dissolved by an aqueous solution (25 vol.%) of HF, without macroscopic evidences of chemical attack of the metal.

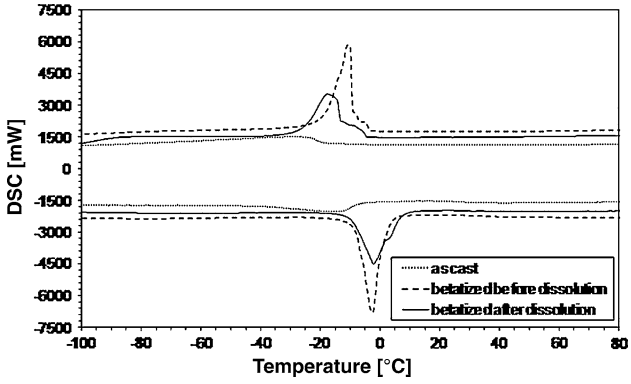


**Fig. 9** DSC profiles of betatized foam specimens

4. The resulting metal foam features a relative density of 0.31 and all the observed cells are open and interconnected.
5. A thermoelastic martensitic transformation on foamed material was observed.
6. The foaming process is practically irrelevant on the transformation temperature of the SMA. In order to clarify possible effects of the chemical etching necessary to dissolve the silica-gel beads, on the functional properties of the material, further study are in progress.

## Acknowledgments

The authors would like to acknowledge Fondazione CARIPLO and the Department of Mechanics of Politecnico di Milano for the financial support, the Department of Engineering Materials of University of Concepción, Prof. W. Nicodemi for his encouragement to the activity of E.M Castrodeza in Italy and Mr. M. Pini for his irreplaceable work during the experimental activities.

## References

1. M.F. Ashby, A. Evans, N.A. Fleck, L. Gibson, J.W. Hutchinson, and H. Wadley, *Metal Foams: A Design Guide*, Butterworth-Heinemann, Boston, 2000
2. J. Banhart, Manufacture Characterization and Application of Cellular Metals and Metal Foams, *Prog. Mater. Sci.*, 2001, **46**(6), p 559–632
3. H.N.G. Wadley, Cellular Metals Manufacturing, *Adv. Eng. Mater.*, 2002, **4**(12), p 726–733
4. J.F. Despois, A. Marmottant, L. Salvo, and A. Mortensen, Spherical Pore Replicated Microcellular Aluminium: Processing and Influence on Properties, *Mater. Sci. Eng. A*, 2007, **462**(1–2), p 68–75
5. E.M. Castrodeza and C. Mapelli, *Italian Industrial Patent Process MO 2008 A 166* (in press)
6. E.M. Castrodeza and C. Mapelli, Processing of Brass Open-cell Foam by Silica-gel Replication, *J. Mater. Process. Technol.*, 2009 (in press)
7. A. Pollien, Y. Conde, L. Pambaguian, and A. Mortensen, Graded Open-cell Aluminium Foam Core Sandwich Beams, *Mater. Sci. Eng. A*, 2005, **404**(1–2), p 9–18
8. C. Gaillard, J.F. Despois, and A. Mortensen, Processing of NaCl Powders of Controlled Size and Shape for the Microstructural Tailoring of Aluminium Foams, *Mater. Sci. Eng. A*, 2004, **374**(1–2), p 250–262
9. A.H. Brothers, R. Scheunemann, J.D. DeFouw, and D. Dunand, Processing and Structure of Open-celled Amorphous Metal Foams, *Scr. Mater.*, 2005, **52**(4), p 335–339
10. H. Funakubo, *Shape Memory Alloys*, Gordon and Breach Science Publishers, Tokyo, 1984
11. K. Otsuka and C.M. Wayman, *Shape Memory Materials*, Cambridge University Press, London, 1998

12. M. Stipcich and R. Romero, The Effect of Post-quench Aging on Stabilization of Martensite in Cu–Zn–Al and Cu–Zn–Al–Ti–B Shape Memory Alloys, *Mater. Sci. Eng. A*, 1999, **273–275**, p 581–585
13. J.L. Pelegrina and M. Ahlers, Stabilization and Ferroelasticity in Cu–Zn Based Martensites, *Scr. Mater.*, 2004, **50**(2), p 213–218
14. M. Ahlers, Stability of Martensite in Noble Metal Alloys, *Mater. Sci. Eng. A*, 2003, **349**(1–2), p 120–131
15. K. Otsuka and X. Ren, Mechanism of Martensite Aging Effect, *Scr. Mater.*, 2004, **50**(2), p 207–212
16. S. Kustov, J. Pons, E. Cesari, and J. Van Humbeeck, Pinning-induced Stabilization of Martensite: Part II. Kinetic Stabilization in Cu–Zn–Al Alloy Due to Pinning of Moving Interfaces, *Acta Mater.*, 2004, **52**(10), p 3083–3096
17. J.A. Giampaoli, J.L. Pelegrina, and M. Ahlers, Ferroelasticity or Rubber Like Behaviour in Stabilized Cu-Zn-Al Single Crystals, *Acta Mater.*, 1998, **46**(10), p 3333–3342
18. R.J. Garcia, Stabilization of Martensite in Cu-Zn-Al Shape Memory Alloys: Effects of γ Precipitates and Thermal Cycling, *Scr. Mater.*, 2000, **42**(6), p 531–536
19. B. Chen, C. Liang, D. Fu, and D. Ren, Corrosion Behavior of Cu and Cu-Zn-Al Shape Memory Alloy in Simulated Uterine Fluid, *Contraception*, 2005, **72**(3), p 221–224
20. F.J. Gil, J.M. Guilemany, and J. Fernandez, Kinetic Grain Growth in Beta-copper Shape Memory Alloys, *Mater. Sci. Eng. A*, 1998, **241**(1–2), p 114–121
21. F.J. Gil and J.M. Guilemany, Effect of Cobalt Addition on Grain Growth Kinetics in Cu-Zn-Al Shape Memory Alloy, *Intermetallics*, 1997, **6**(5), p 445–450
22. S.A. Lermontov and A.N. Malkova, A New Method for Dissolution of Silica Gel in a Pentafluoropropionyl Fluoridetertiary Amine System, *Russian Chem. Bull.*, 2007, **56**(3), p 435–437
23. G. Spierings, Wet Chemical Etching of Silicate Glasses in Hydrofluoric Acid Based Solutions, *J. Mater. Sci.*, 1993, **28**(23), p 6261–6273
24. A.J. Matheson, Computation of a Random Packing of Hard Spheres, *J. Phys. C Solid State Phys.*, 1974, **7**(15), p 2569–2576
25. A. Donev, S. Torquato, F.H. Stillnger, and R. Cornelly, Jamming in Hard Sphere and Disk Packings, *J. Appl. Phys.*, 2004, **95**(3), p 989–999